Electronic Supplementary Material (ESI) for Nanoscale.

Supplementary Information

Simple Synthesis of Vacancy-Rich NiO 2D/3D Dendritic Self-Supported Electrode for Efficient Overall Water Splitting

Renjie Ji[a*], Fan Zhang[a*], Yonghong Liu[a, b†], Yuan Pan[c], Zhijian Li[a], Zheng Liu[a], Shuaichen Lu[a], Yating Wang[a], Hang Dong[a], Peng Liu[a], Xinlei Wu[a], Hui Jin[a]

[a] College of Mechanical and Electronic Engineering, China University of Petroleum (East China), Qingdao 266580, PR China.

[b] Key Laboratory of Unconventional Oil & Gas Development, China University of Petroleum (East China), Ministry of Education, Qingdao, PR China.

[c] State Key Laboratory of Heavy Oil Processing, Key Laboratory of Catalysis, China University of Petroleum (East China), Qingdao 266580, PR China.

†Corresponding author. Email: liuyhupc@126.com (Yonghong Liu)

*These authors contributed equally to this work and should be considered as the co-first authors.

Experimental Section

Chemicals

All reagents (AR) were purchased from Sinopharm Chemical Reagent Co. Ltd. without further purification. The commercial catalysts of 20 wt% Pt/C and irdium(IV) oxide (IrO_2, 99.9%) were purchased from Aladdin Chemical Co. Ltd. Nickel foam (NF) with a thickness of 1.6 mm was purchased from Jiangsu Jiayisheng Metal Foam Co. Ltd. Titanium plate and rods were purchased from Shenzhen Hongwang Co. Ltd. Deionized water (resistance of 18.2 MΩ) was used in all experiments.

Preparation of the dendritic self-supported skeleton (DSS)

The DSS was prepared by regional cathodic electrodeposition of Ni on the titanium (Ti) plate. The Ti plate (3cm×3cm) that was used as the cathode was first rinsed with acetone and ethanol in an ultrasonic bath for 10min and then washed thrice with deionized water before use. The Ti rod with 6mm diameter was applied as the anode. Electrodeposition was carried out with a vertical-electrode configuration in a cell containing $NiSO_4 \cdot 6H_2O$ (300 g/l), $NiCl_2 \cdot 6H_2O$ (40 g/l) and H_3BO_3 (40 g/l) at room temperature. The Ti rod was installed on the z-direction slideway, and the Ti plate was laid in the tank within a distance of 1 mm between the end face of graphite rod and Ti plate. Electrodeposition was performed at a constant voltage of 6 V for 30 min with the z-direction movement of the slideway by automatically controlled by a computer. Finally, the DSS was removed from Ti plate and flattened. The prepared DSS was washed with ethanol and deionized water and dried in an oven at 60 °C for 12 h.

Preparation of the NiO-Vo@2D/3D NS@DSE

From above process, the DSS can be relaxed to clip and spread as a plate-type electrode with an area of ≈1 cm^2. Afterword, the plate-type DSS was immersed in 2 M HCl solution for 20 min at 90 °C to allow for the in situ etching and oxidation, giving rise to the formation of 2D NiO nanosheets adhering to 3D nanospheres. Finally, the NiO-Vo@2D/3D NS@DSE was removed and repeatedly flushed with large volumes of water and ethanol, respectively. Then, the NiO-Vo@2D/3D NS@DSE was dried at 60 °C for 24 h.

Material Characterization

The morphology of samples and element distributions were characterized by scanning electron microscopy (SEM; Zeiss Merlin Compact with energy dispersive X-ray spectroscopic (EDS)).

Transmission electron microscopy (TEM) and high-resolution TEM were performed by JEOL-2100F system with 200 kV working voltage. X-ray diffraction was performed using an X′Pert PRO MPD with a Cu K_α source. The element valence states were measured by X- ray photoelectron spectroscopy (Thermo Scientific ESCALAB 250XI) with a 150 W Al K_α photon source. The catalyst mass was measured by Sartorius analytical balance (GL124-1SCN) with resolution ratio of 0.1 mg. Atomic force microscopy (SPM-9700) was utilized to measure the thickness of 2D nanosheets on the 3D NiO nanosphere. N_2 absorption/desorption analysis was performed on a MicroActive for ASAP 2420 analyzer at -196 ℃ (77K). Brunauer-Emmett-Teller and Barrett-Joyner-Halenda methods were used to calculate the specific surface area and pore size of the samples, respectively. Ni K-edge X-ray absorption fine-structure spectra were obtained at 1W1B station in Beijing Synchrotron Radiation Facility (P. R. China) operated at 2.5 GeV with a maximum current of 250 mA. Electron paramagnetic resonance (EPR) were measured by a Bruker A300 EPR spectrometer. The metal elemental analysis via inductively coupled plasma optical emission spectroscopy of the solution was performed on Agilent 730ES. Fourier transform infrared spectroscopy (FTIR) was recorded on a Bruker Vertex70.

Electrochemical measurements

All the electrochemical measurements were performed by using a CHI 760E electrochemical workstation in a standard three electrode system using graphite and saturated calomel electrode (SCE) as the count and reference electrodes, respectively. All the potentials measured were calibrated to reversible hydrogen electrode (RHE) via the following equation: $E_{RHE}=E_{SCE}+1.06$ V (Figure S1). The polarization curves were carried out with the scan rate of 2 mV/s. The electrode with 20%Pt/C and IrO_2 was fabricated by dispersing the catalysts in the 480 μl ethanol, 480μl deionized water and 40 μl 20% Nafion solution by ultrasonication for 30 min. Then, the ink was uniformly coated on the samples (0.5 cm^2) to load a catalyst mass of approximately 2 mg/cm^2 after drying. The as-prepared sample was used directly as the work electrode in the 1 M KOH solution. The O_2-saturated and N_2-saturated process is used before the OER and HER tests, respectively. The long-term test was carried out by the chronoamperometry method at 10 mA/cm^2 with 24 h and cyclic voltammetry (CV). The electrochemical active surface areas (ECSA) was tested by cyclic voltammetry at a varing scan rates of 50, 100, 150, 200, and 250mV/s. Electrochemical impedance spectroscopy (EIS) was performed in the frequency range from 0.1 Hz to 100 kHz. All the unspecified potential curves were IR-corrected. The turnover frequency (TOF) for OER and HER was estimated using the following equation: TOF= jM/4Fm and TOF= jM/2Fm, where j is the current density, F is Faraday's constant (96485.3 C/mol), M is the molar mass, m is the loading mass, and numbers 4 and 2 means 4 and 2 electrons per mole of O_2 and H_2, respectively. Meanwhile, the Faradic efficiency was calculated by the equation, Faradic efficiency=nFm/Q, where n equals 2 and 4 for HER and OER respectively, F is Faraday's constant (96485.3 C/mol), m is moles of gas evolved and Q is the total charge passed.

Density functional theory (DFT) Calculations

All the DFT calculations were performed by Vienna Ab-initio Simulation Package (VASP) [1, 2], employing the Projected Augmented Wave[3] (PAW) method. The revised Perdew-Burke-Ernzerhof (RPBE) functional was used to describe the exchange and correlation effects [4-6]. The GGA + U calculations are performed using the model proposed by Dudarev et al.[7], with the U_{eff} (U_{eff} = Coulomb U–exchange J) value of 6.4 eV for Ni. The surface models were constructed by using a 3×3 supercell. For all the geometry optimizations, the cutoff energy was set to 450 eV. A 3×3×1 Monkhorst-Pack grid[8] was used to carry out the surface calculations on all the models. At least 20 Å vacuum layer was applied in the z-direction of the slab models, preventing the vertical interactions between slabs.

In alkaline conditions, OER could occur in the following four elementary steps:

$$OH^- + * \rightarrow *OH + e^-$$

$$*OH + OH^- \rightarrow *O + H_2O + e^-$$

$$*O + OH^- \rightarrow *OOH + e^-$$

$$*OOH + OH^- \rightarrow * + O_2 + H_2O + e^-$$

where * denotes the active sites on the catalyst surface.

For the hydrogen evolution reaction (HER) in alkaline condition, the mechanism involving two reaction intermediates are calculated:

$$H_2O + * \rightarrow *H\text{–}OH$$

$$H* \rightarrow 1/2\ H_2 + *$$

In this mechanism, water dissociated into an adsorbed H-OH state at the catalyst surface, making *H-OH the first reaction intermediate. Thereafter, the adsorbed OH dissolved into the solution, and the adsorbed H combines with an electron and proton pair to form the gaseous hydrogen molecule.

The computational hydrogen electrode (CHE) model[9] was used to calculate the free energies of OER and HER, based on which the free energy of an adsorbed species is defined as

$$\Delta G_{ads} = \Delta E_{ads} + \Delta E_{ZPE} - T\Delta S_{ads}$$

where ΔE_{ads} is the electronic adsorption energy, ΔE_{ZPE} is the zero point energy difference between adsorbed and gaseous species, and $T\Delta S_{ads}$ is the corresponding entropy difference between these two states. The electronic binding energy is referenced as $1/2H_2$ for each H atom, and (H_2O–H_2) for each O atom, plus the energy of the clean slab. The corrections of zero point energy and entropy of the OER and HER intermediates can be found in the Table S1.

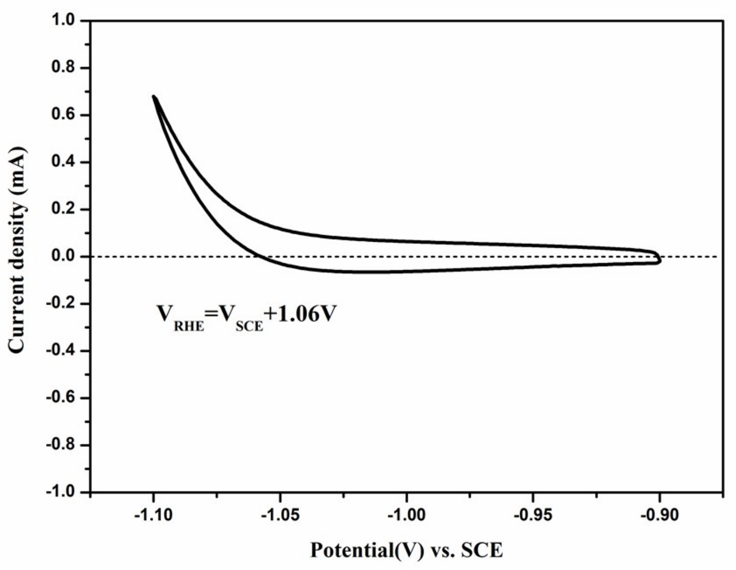

Figure S1 Calibration of the reference saturated calomel electrode (SCE).

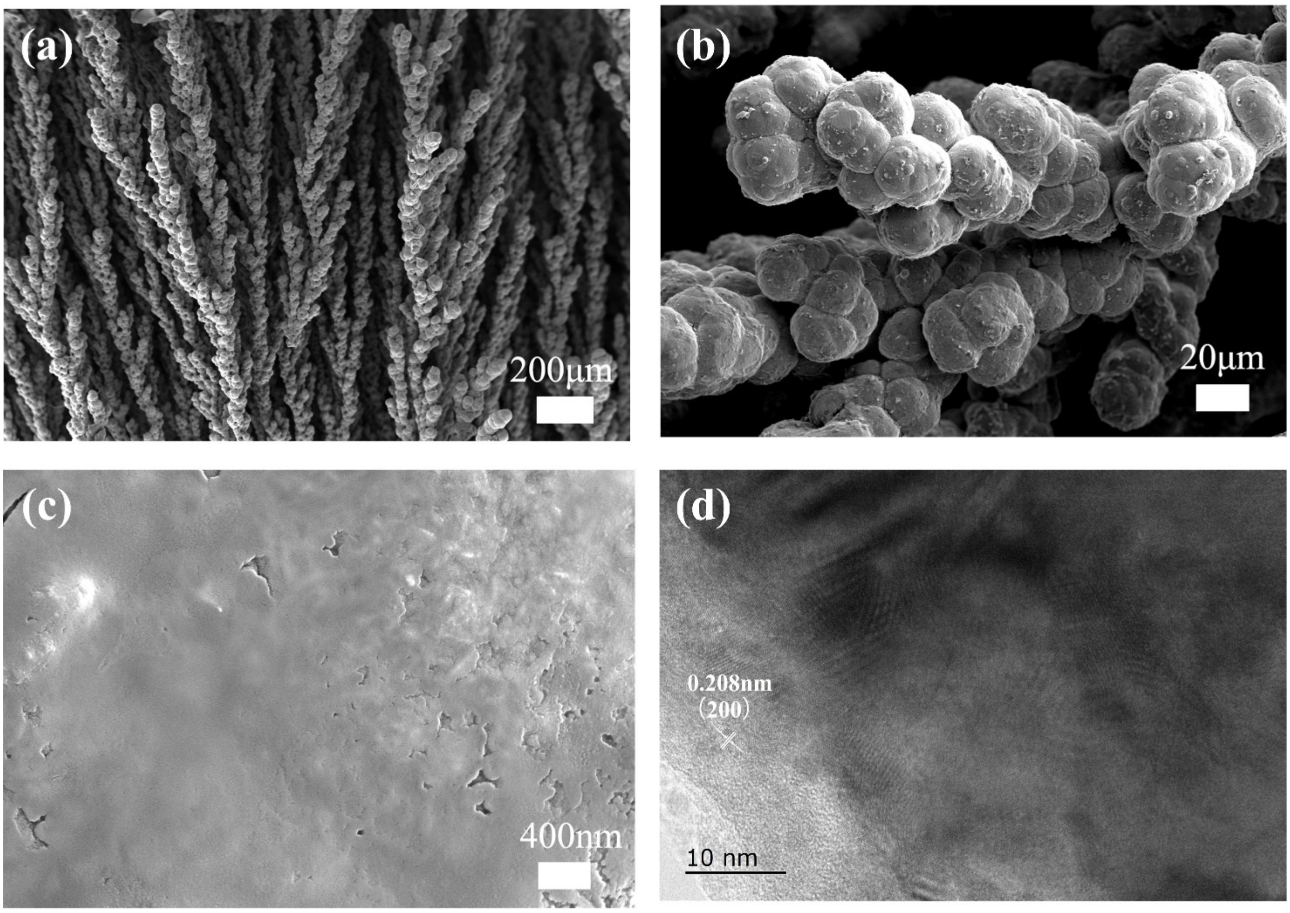

Figure S2 a-c) SEM images of DSS; d) HRTEM image of DSS.

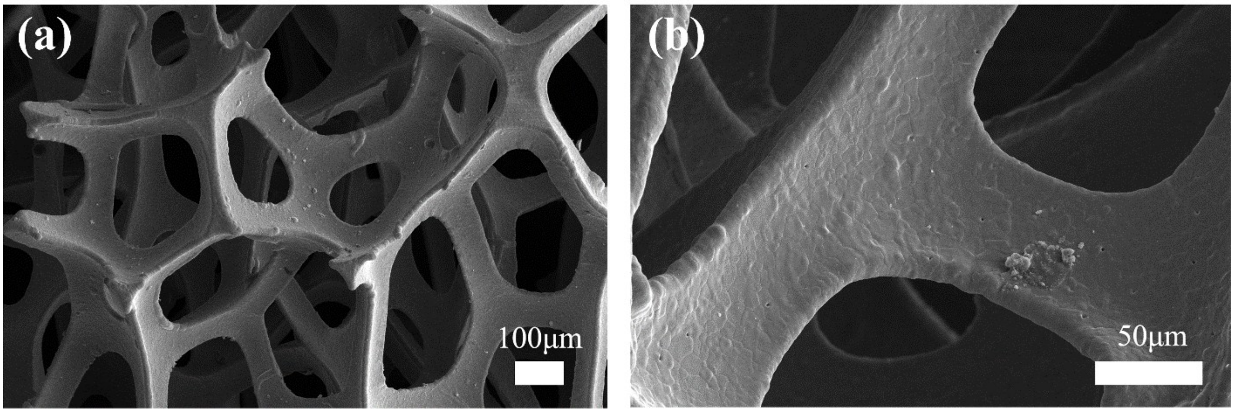

Figure S3 a,b) SEM images of NF.

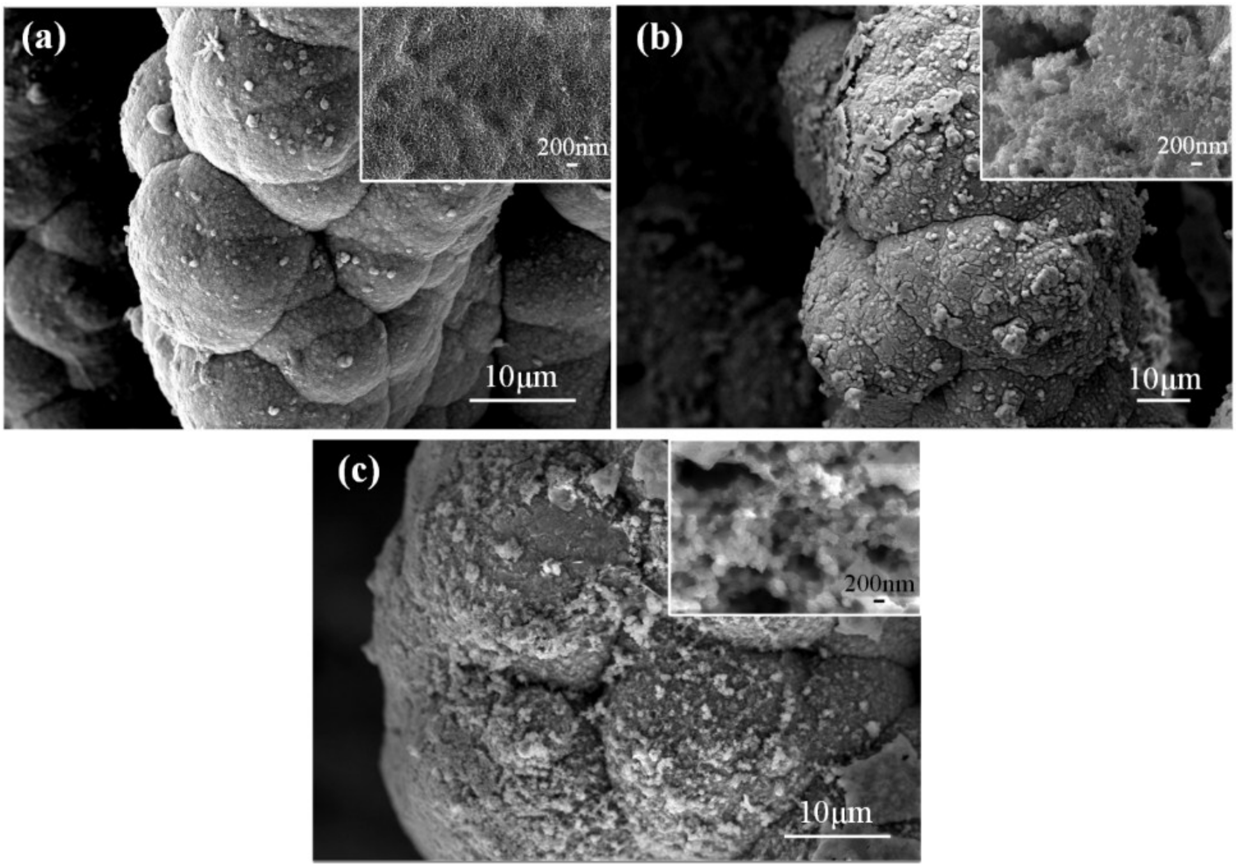

Figure S4 Surface morphologies of a) 30 ℃, b) 50 ℃, and c) 70 ℃ in 2 M HCl solution.

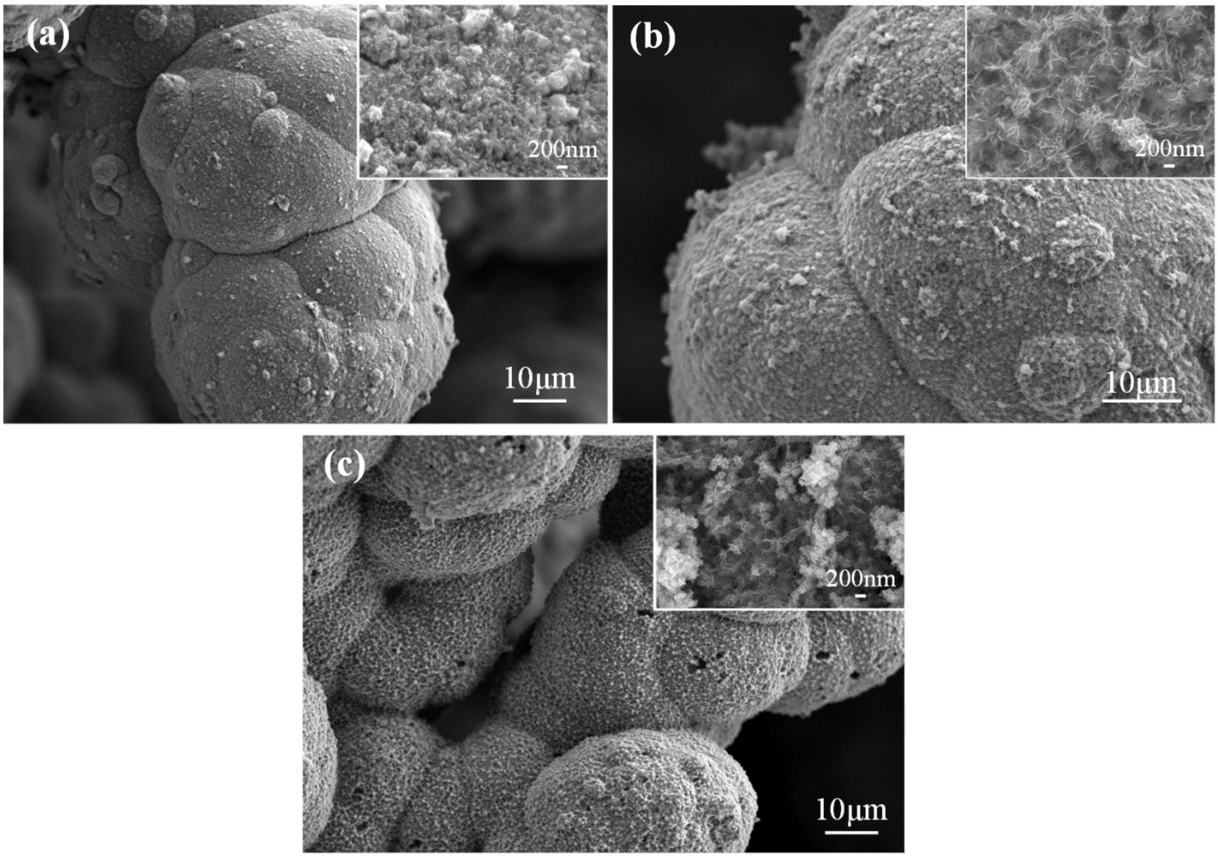

Figure S5 Surface morphologies of in a) 0.5 M, b) 1 M, c) 3 M at 90 ℃ HCl solution.

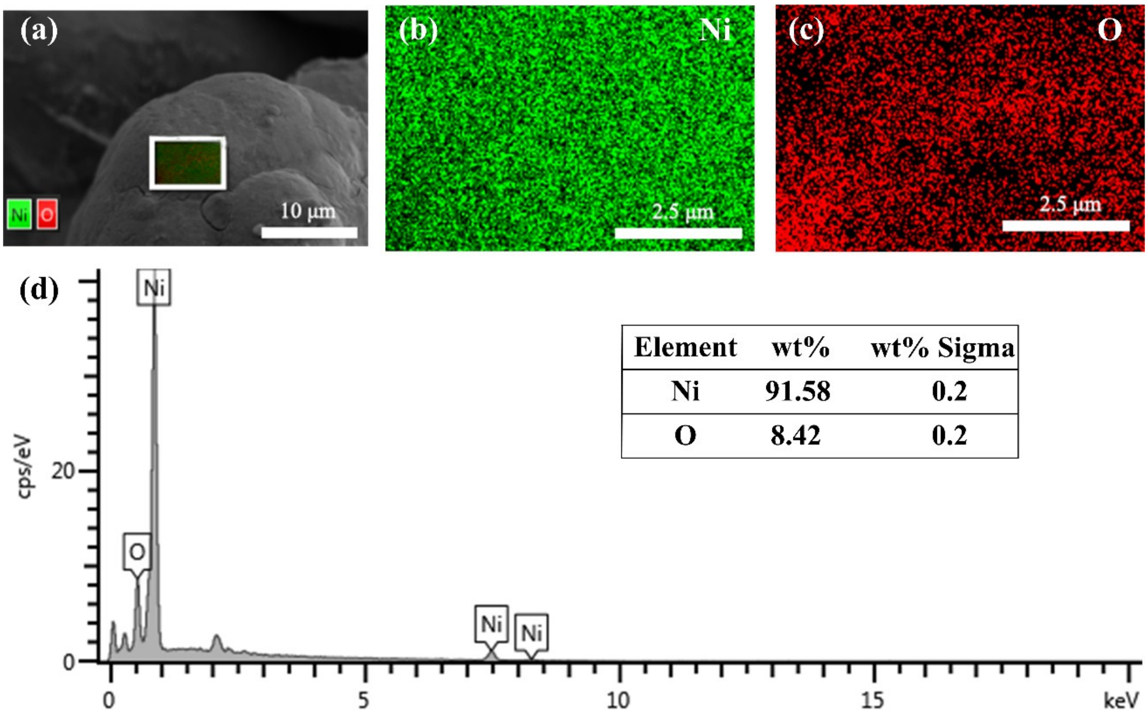

Element	wt%	wt% Sigma
Ni	91.58	0.2
O	8.42	0.2

Figure S6 a-c) EDS mapping of DSS d) EDS pattern of DSS with the weight ratios for elements (inset).

The peaks around 2 keV in the EDS spectra is attributed to Pt, which originated from the sample preparation for SEM by spraying Pt[10].

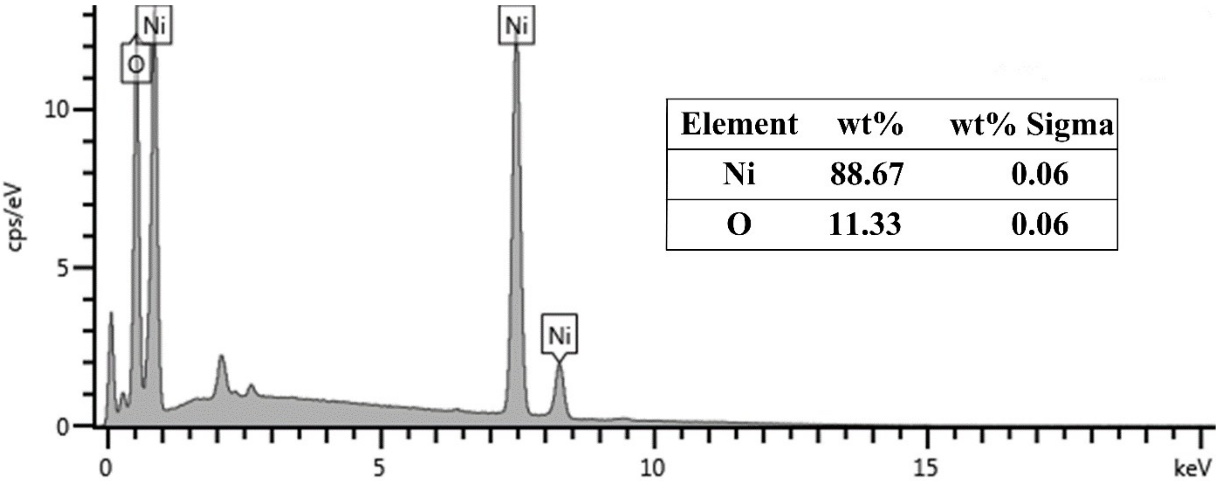

Element	wt%	wt% Sigma
Ni	88.67	0.06
O	11.33	0.06

Figure S7 EDS pattern of the NiO-Vo@2D/3D NS@DSE with the weight ratio for elements (inset). The peaks at around 2 keV in the EDS spectra are as same as those in Figure S4, which was from the sample preparation for SEM by spraying Pt.

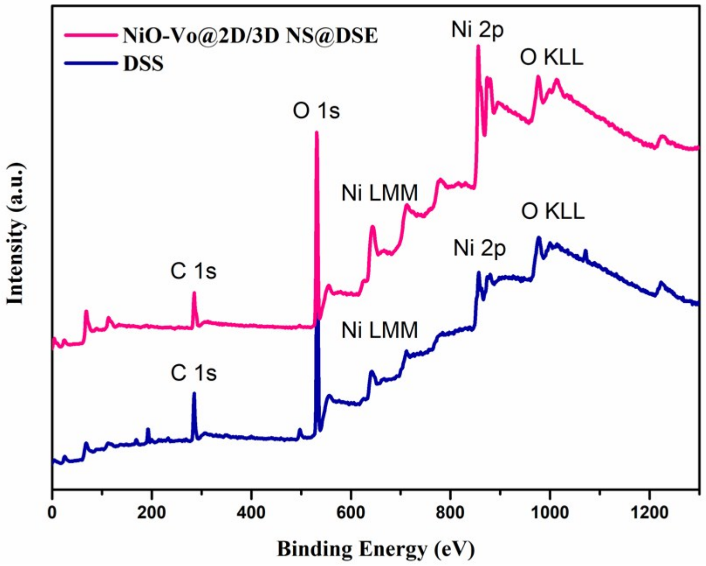

Figure S8 XPS survey spectra.

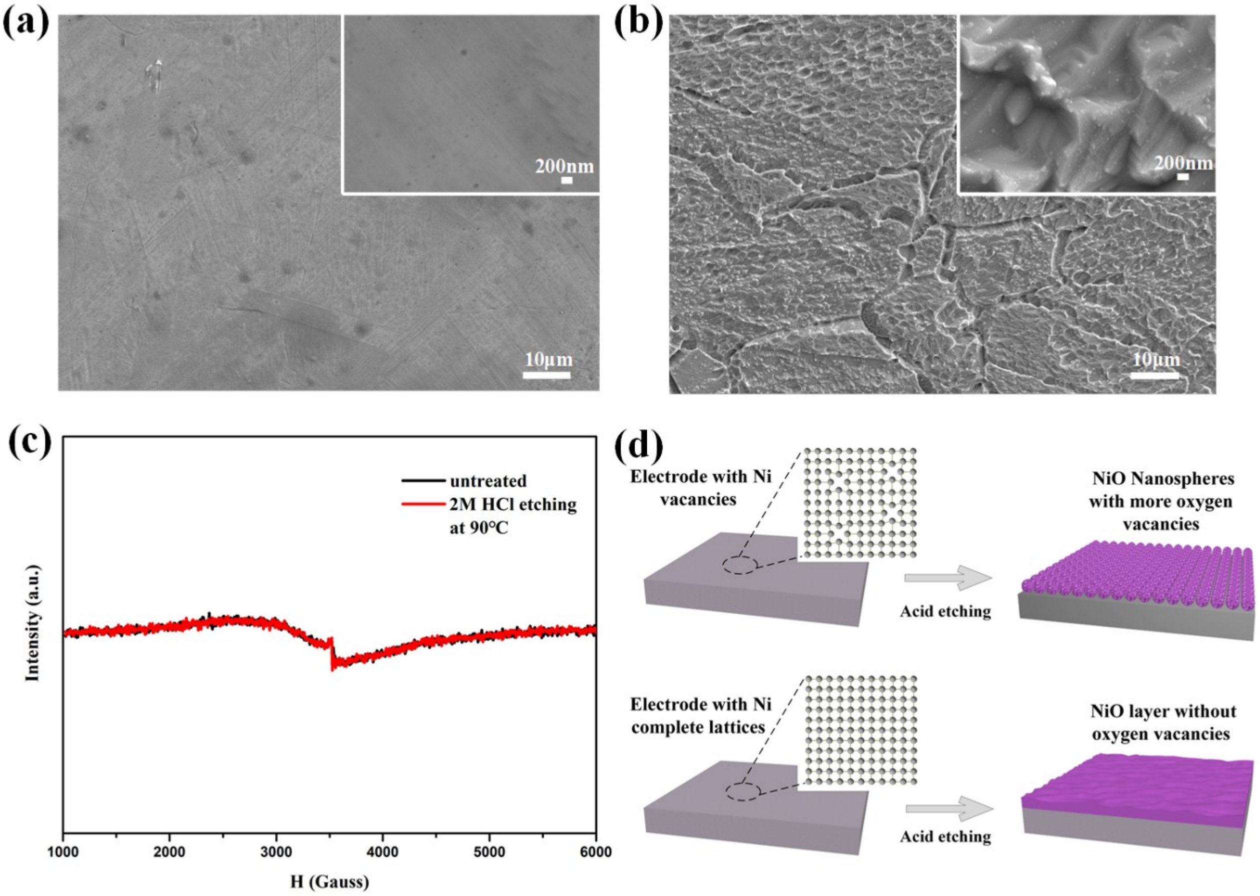

Figure S9 SEM images of Ni foil a) without treatment and b) with etching. c) EPR spectra of Ni foil without treatment and with etching. d) Schematic for the mechanism of oxygen vacancy formation.

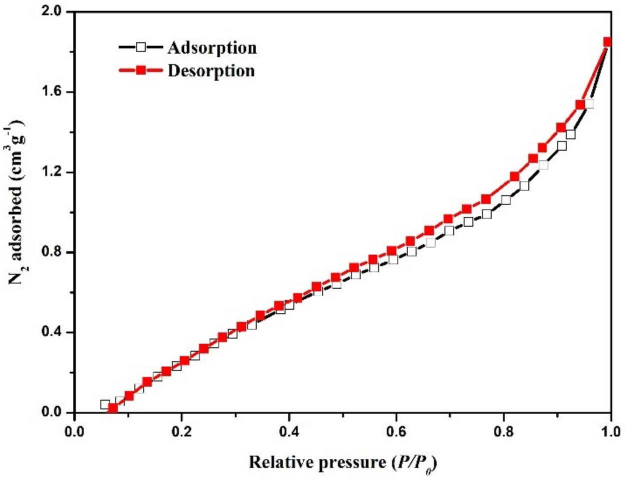

Figure S10 N_2 adsorption/desorption isotherms of DSS

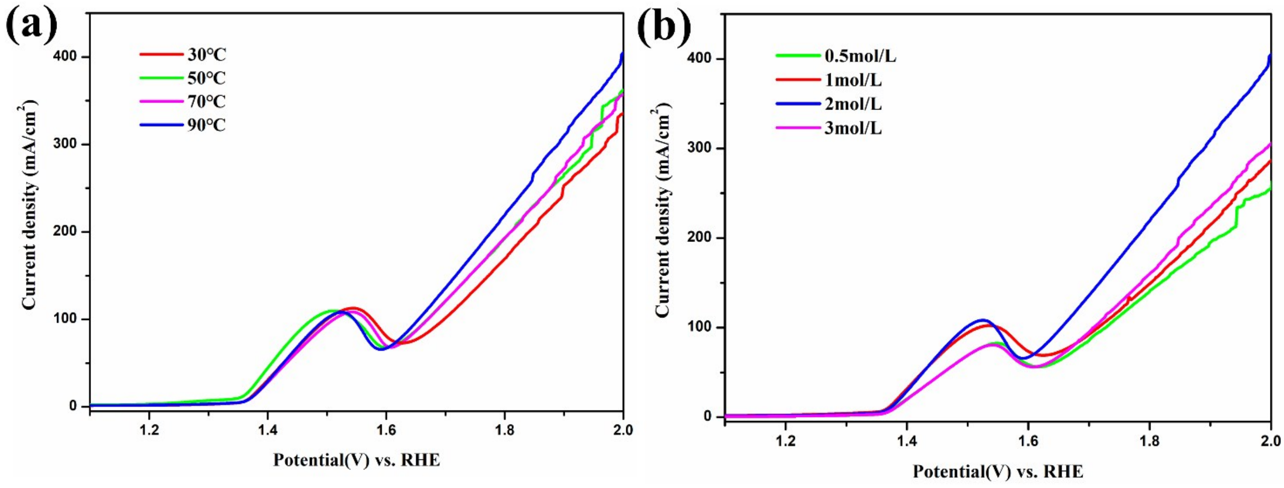

Figure S11 Electrode OER performance without IR compensation. a) Polarization curves for OER in 2 M HCl solution at different temperatures; b) Polarization curves for HCl solution concentrations at 90 ℃.

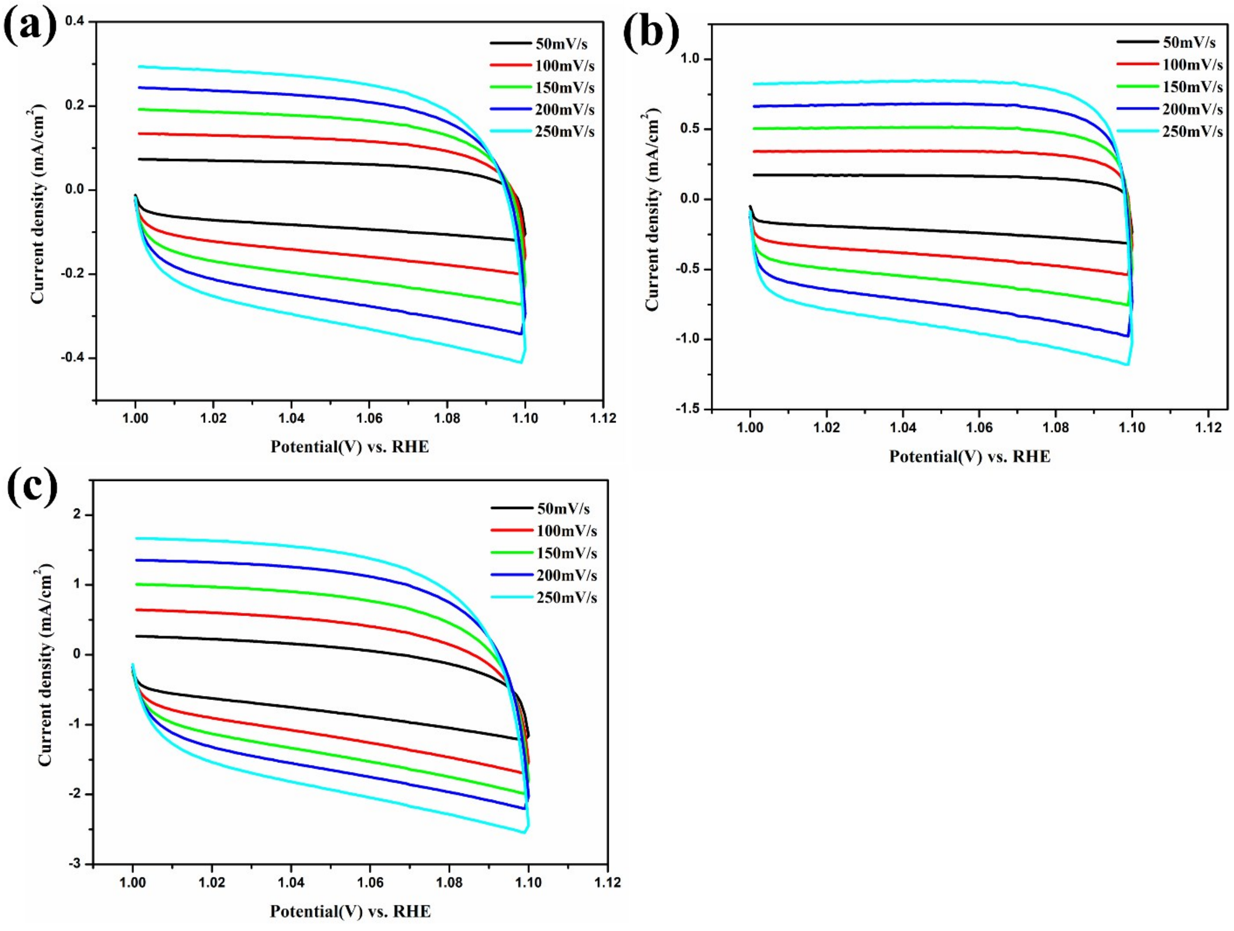

Figure S12 Cyclic voltammograms in the range of 1.0-1.1 V vs RHE. a) NF; b) DSS; c) NiO-Vo@2D/3D NS@DSE.

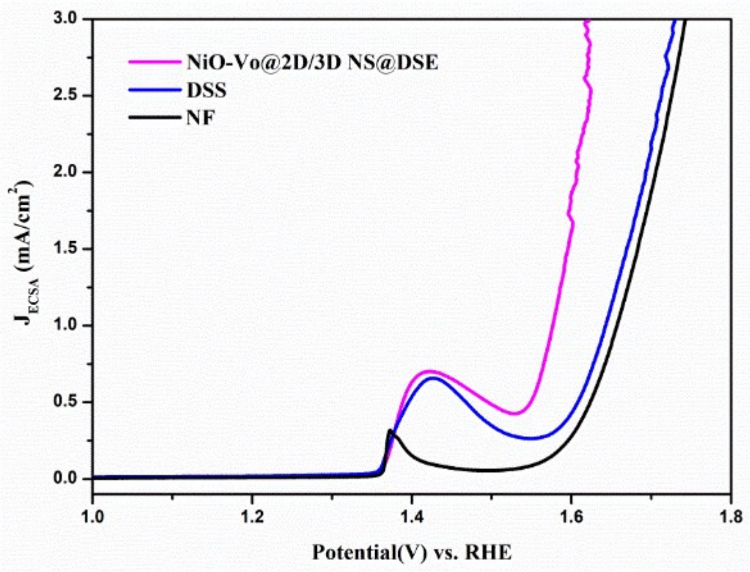

Figure S13 OER polarization curves normalized to the ECSAs for NiO-Vo@2D/3D NS@DSE, DSS and NF.

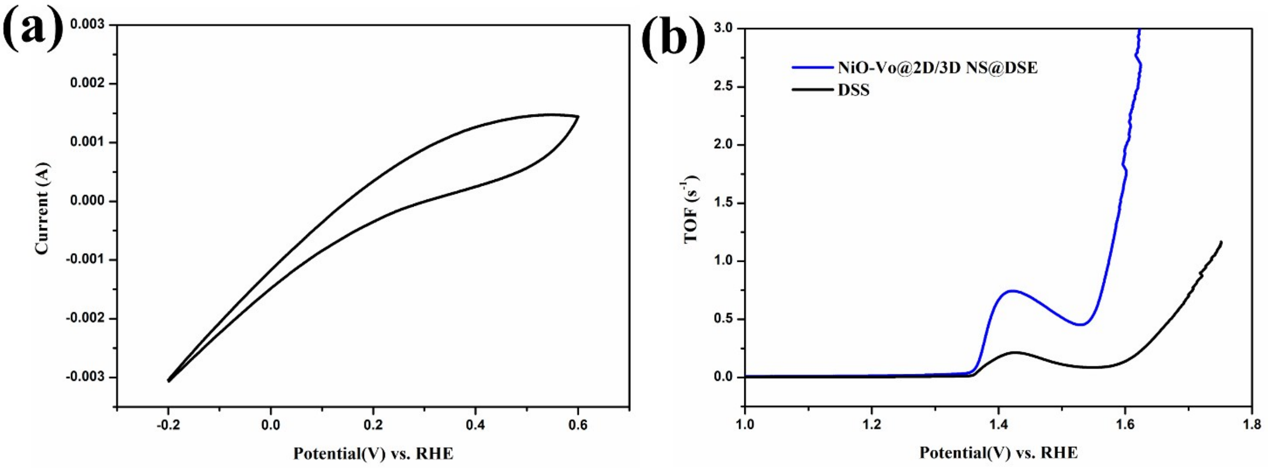

Figure S14 a) CV of 2D/3D NiO DSE in 1 M PBS with a scan rate of 50 mV/s b) TOF of NiO-Vo@2D/3D NS@DSE and DSS for OER.

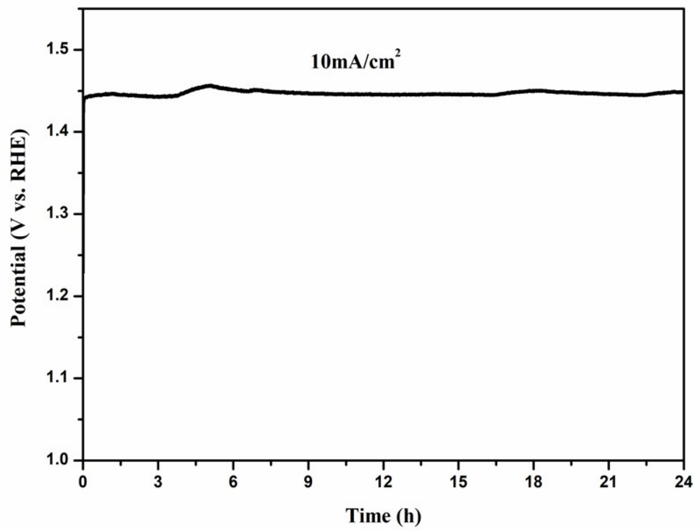

Figure S15 The long-time durability tests at the current density of 10 mA/cm^2.

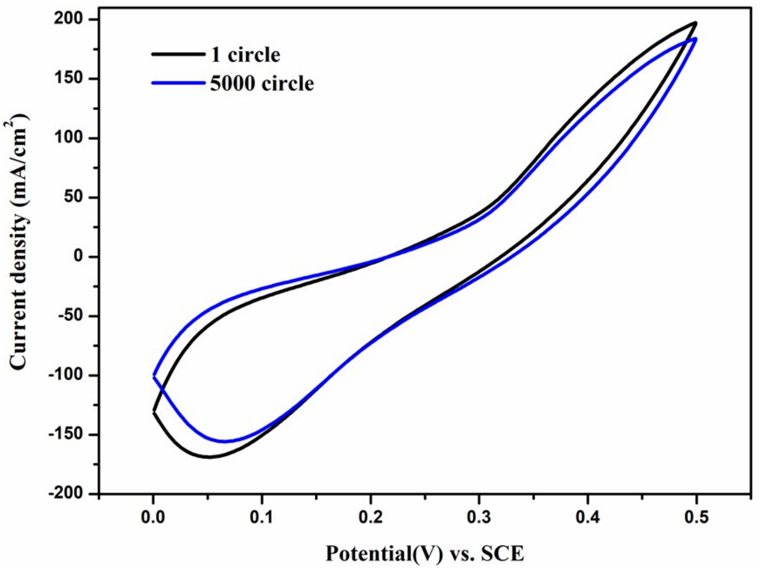

Figure S16 The OER CV measurement curves for durability continuous 5000 cycles.

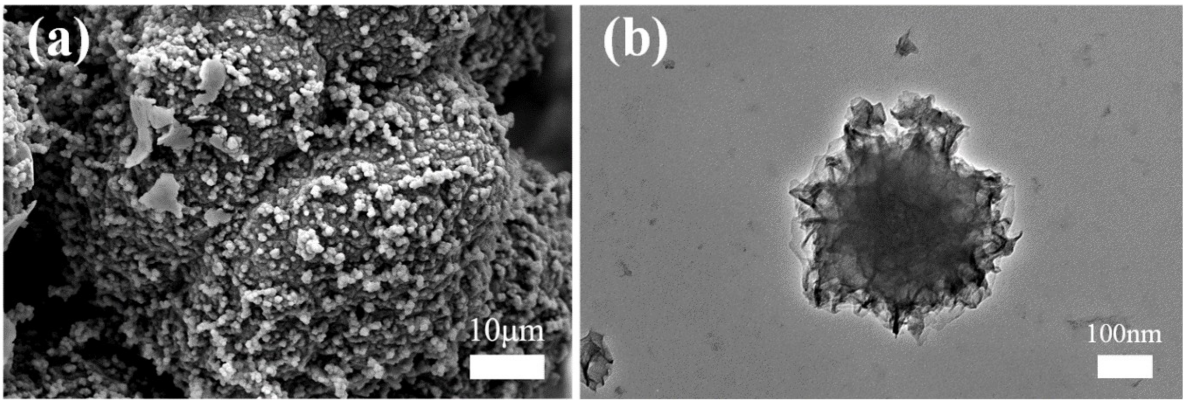

Figure S17 a) SEM and b) TEM images of NiO-Vo@2D/3D NS@DSE for microtopography after 24 h OER reaction.

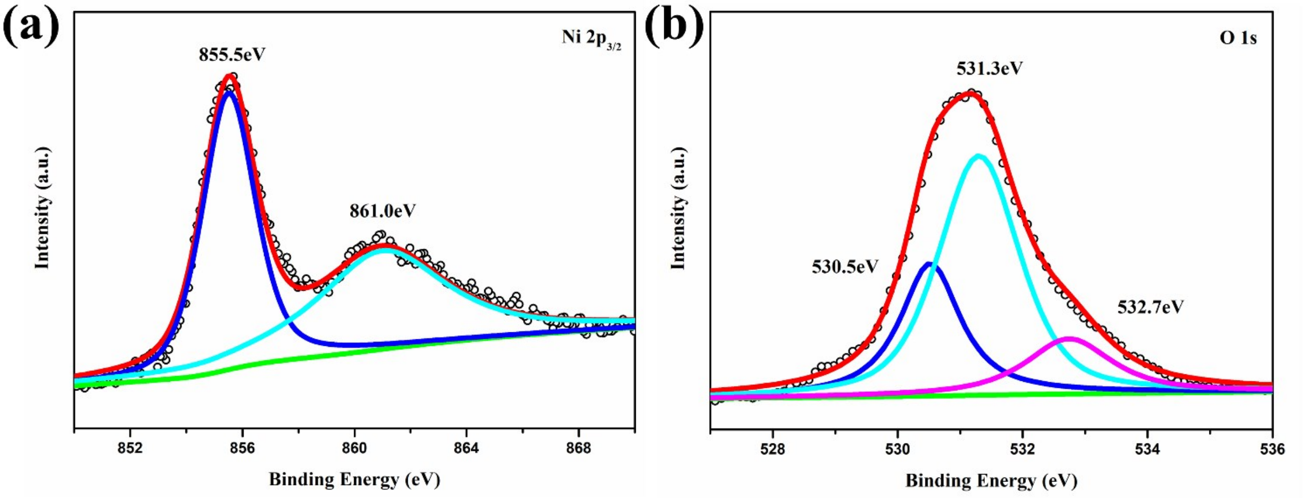

Figure S18 XPS patterns of NiO-Vo@2D/3D NS@DSE after 24 h OER. a) XPS spectra of Ni $2p_{3/2}$; b) XPS spectra of O 1s.

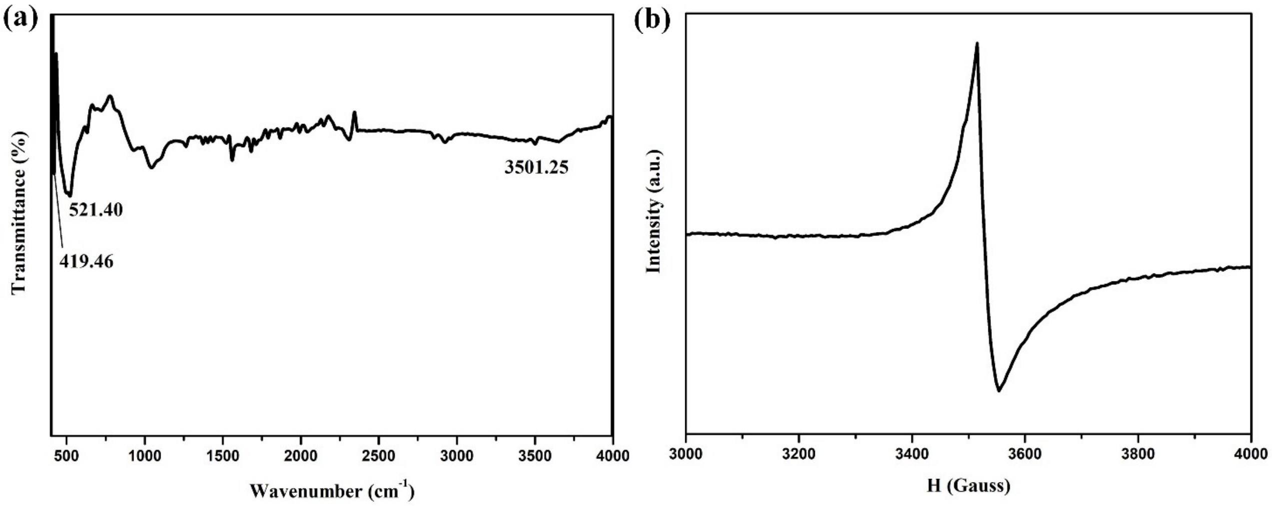

Figure S19 a) FTIR spectrum and b) EPR spectra after OER long-term stability.

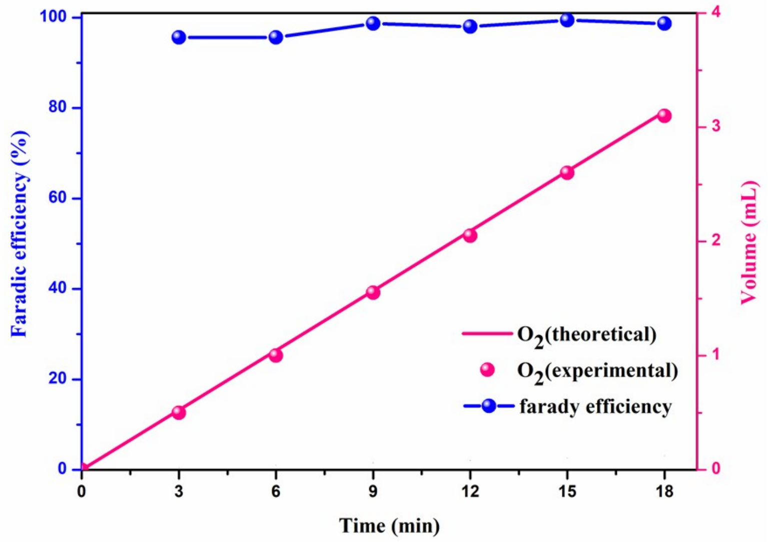

Figure S20 The amount of evolved oxygen and gas at 50 mA cm^{-2} with the faraday efficiency.

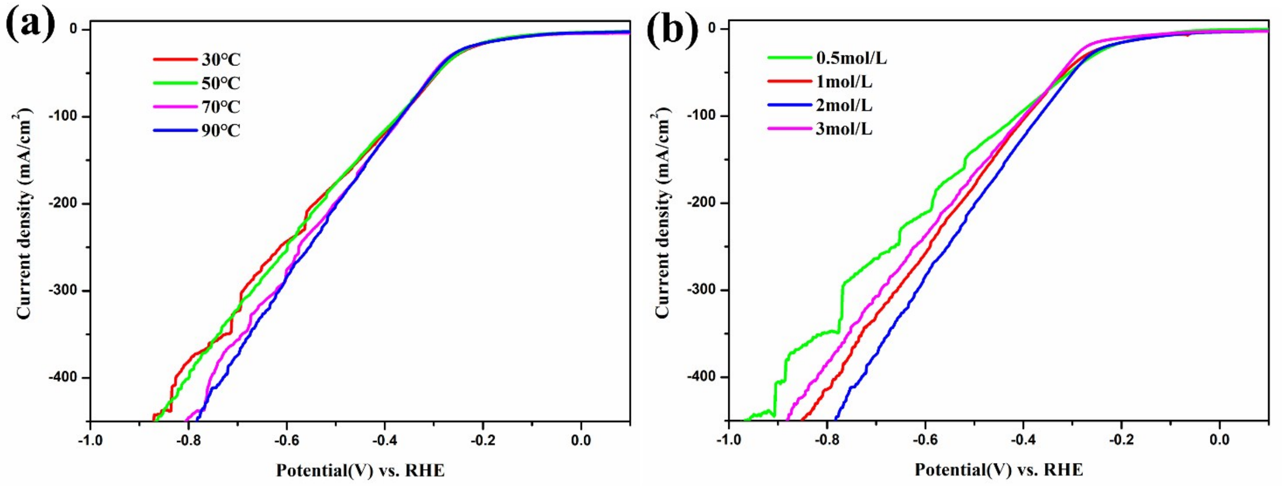

Figure S21 Electrode HER performance without IR compensation. a) Polarization curves of for HER in 2 M HCl solution at different temperatures; b) Polarization curves for HER in different HCl solution concentrations at 90 ℃.

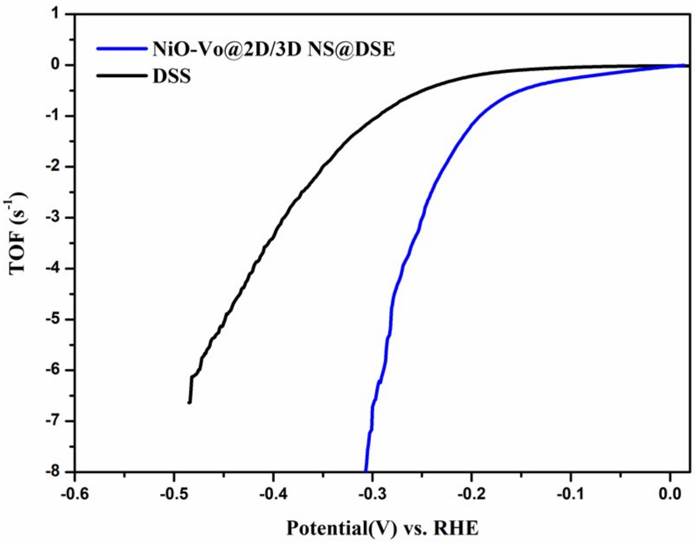

Figure S22 TOF of NiO-Vo@2D/3D NS@DES and DSS for HER.

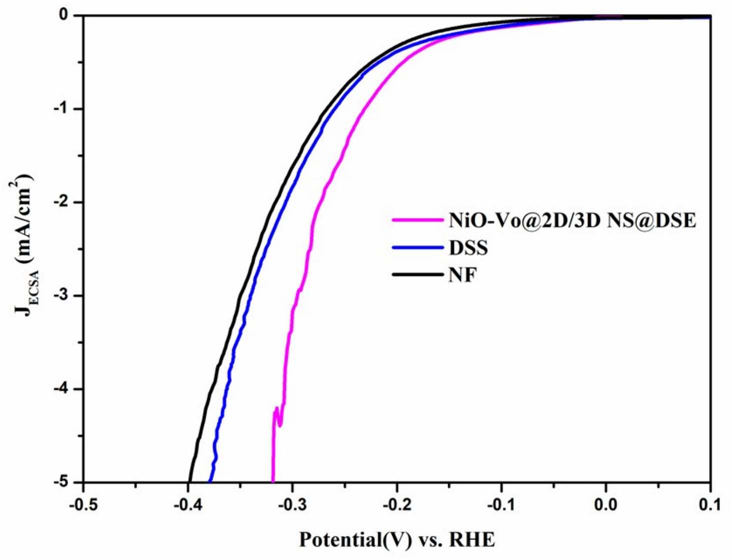

Figure S23 HER polarization curves normalized to the ECSAs for NiO-Vo@2D/3D NS@DSE, DSS and NF.

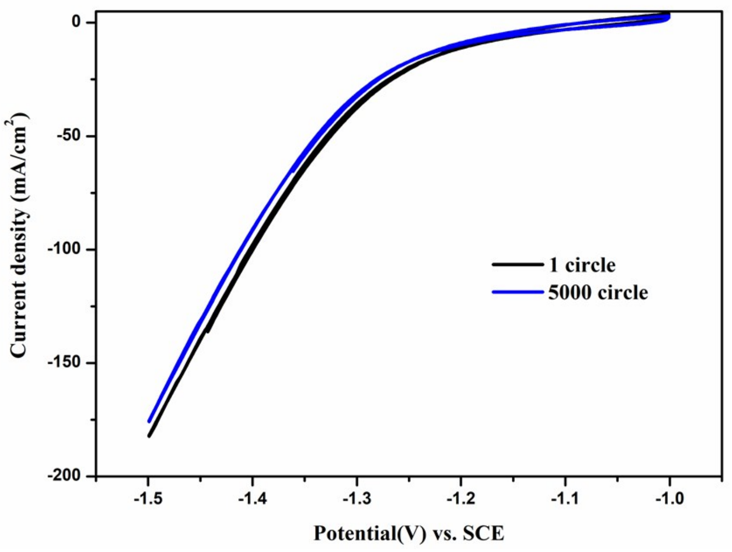

Figure S24 The HER CV measurement curves for durability under continuous 5000 cycles.

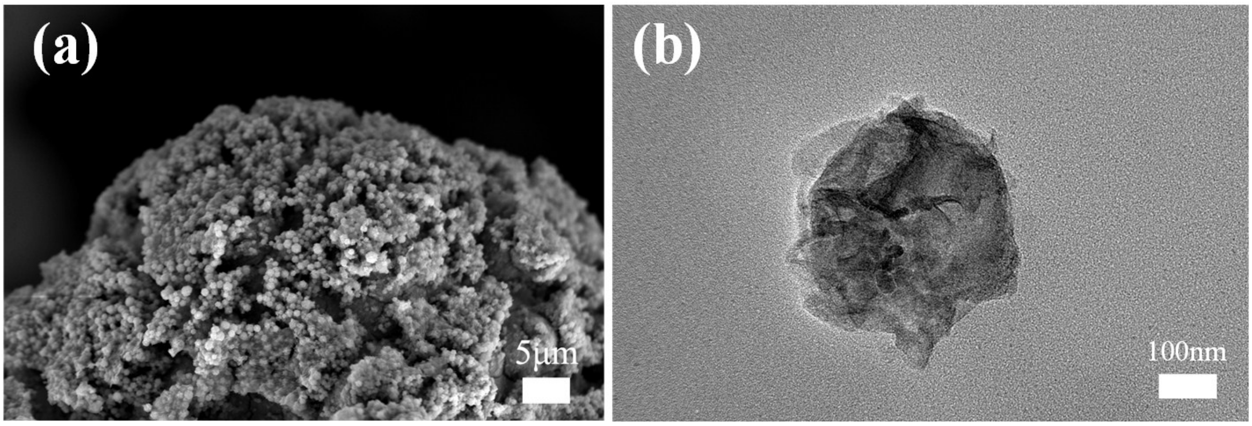

Figure S25 a) SEM and b) TEM images of NiO-Vo@2D/3D NS@DSE for microtopography after 24 h HER reaction.

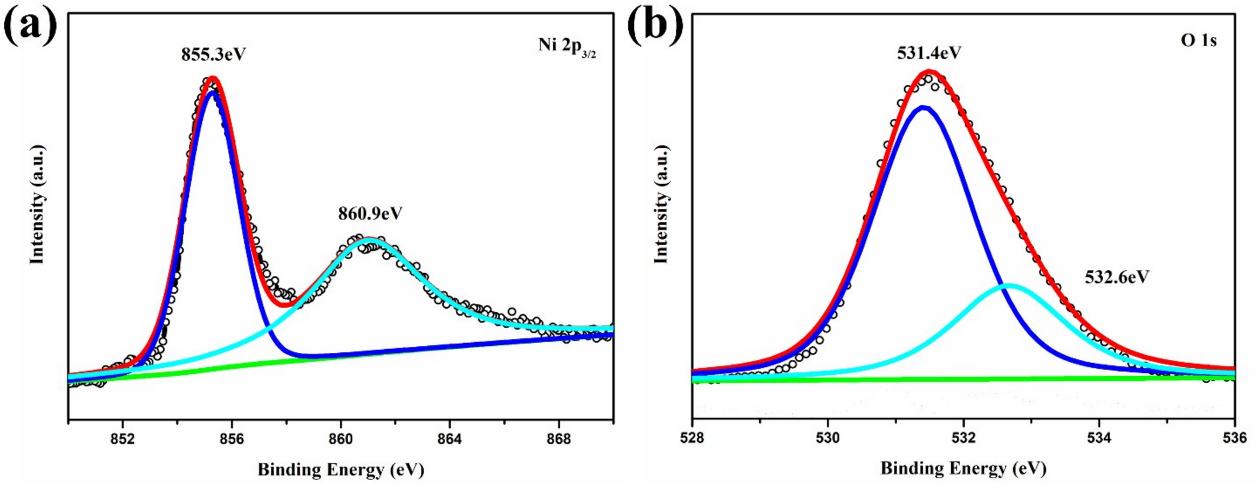

Figure S26 XPS patterns of NiO-Vo@2D/3D NS@DSE after 24 h HER reaction a) XPS spectra of Ni $2p_{3/2}$; b) XPS spectra of O 1s.

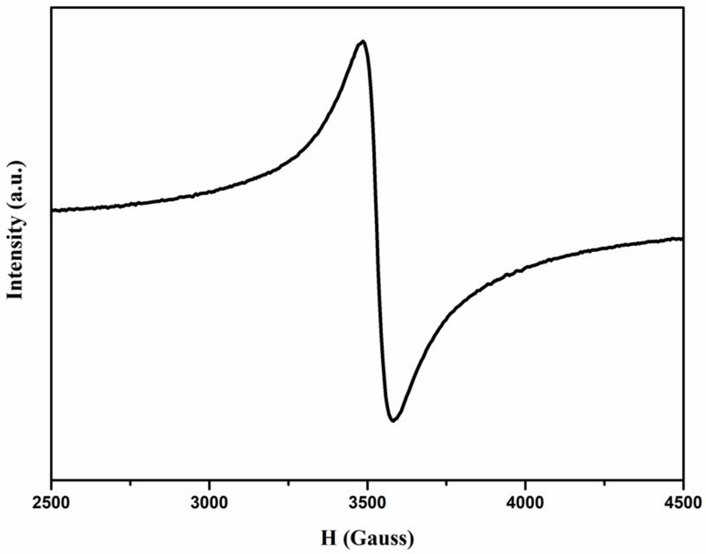

Figure S27 EPR spectra after HER long-term stability test.

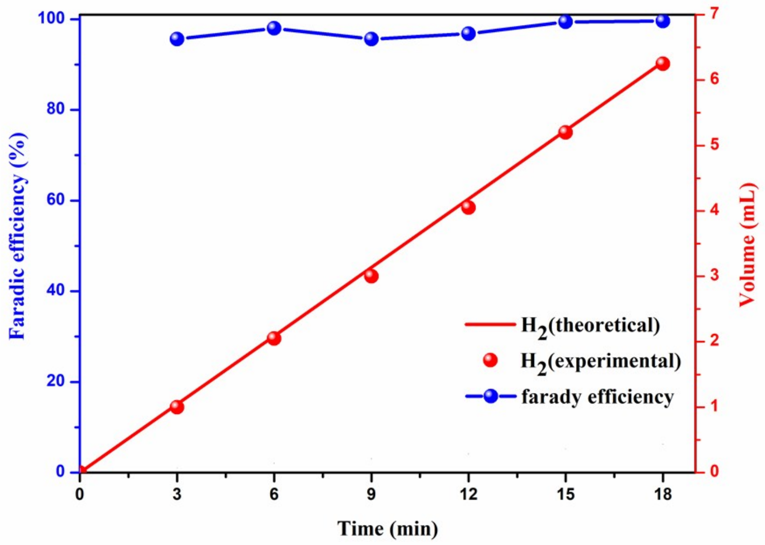

Figure S28 The amount of evolved hydrogen and gas at -50 mA cm^{-2} with faraday efficiency.

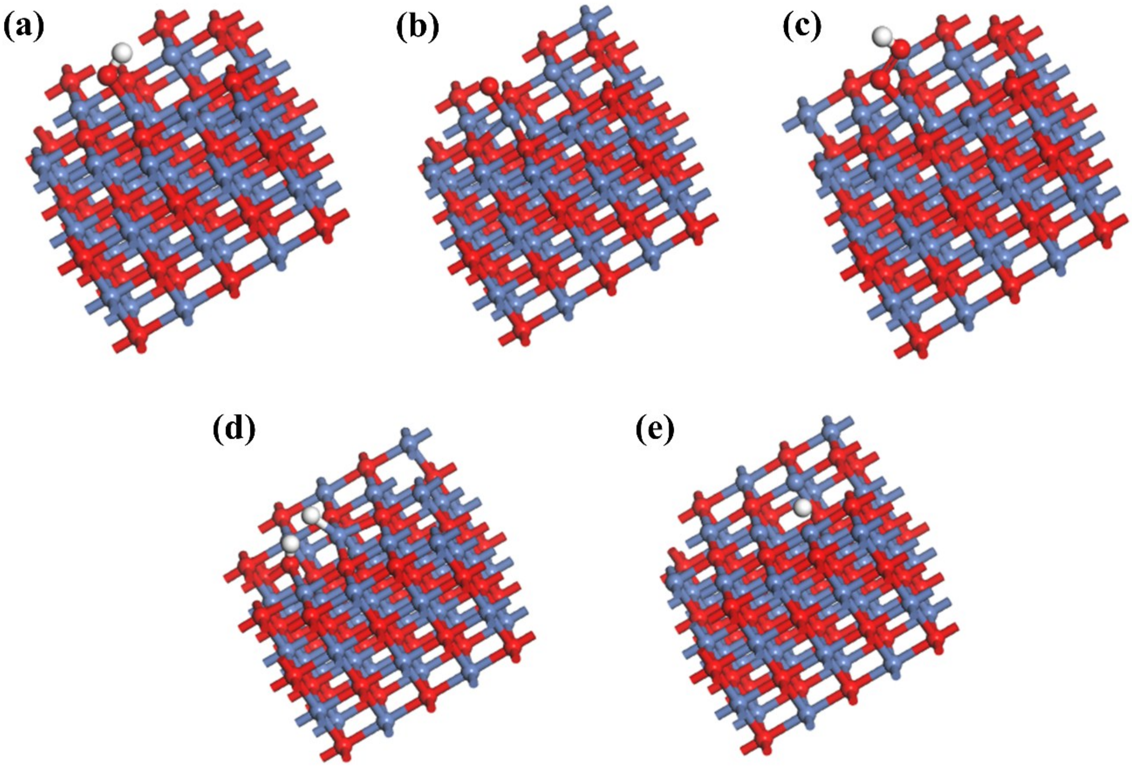

Figure S29 DFT models of NiO-Vo for a-c) OER with OH*, O* and OOH*, d,e) HER with H-OH and H*.

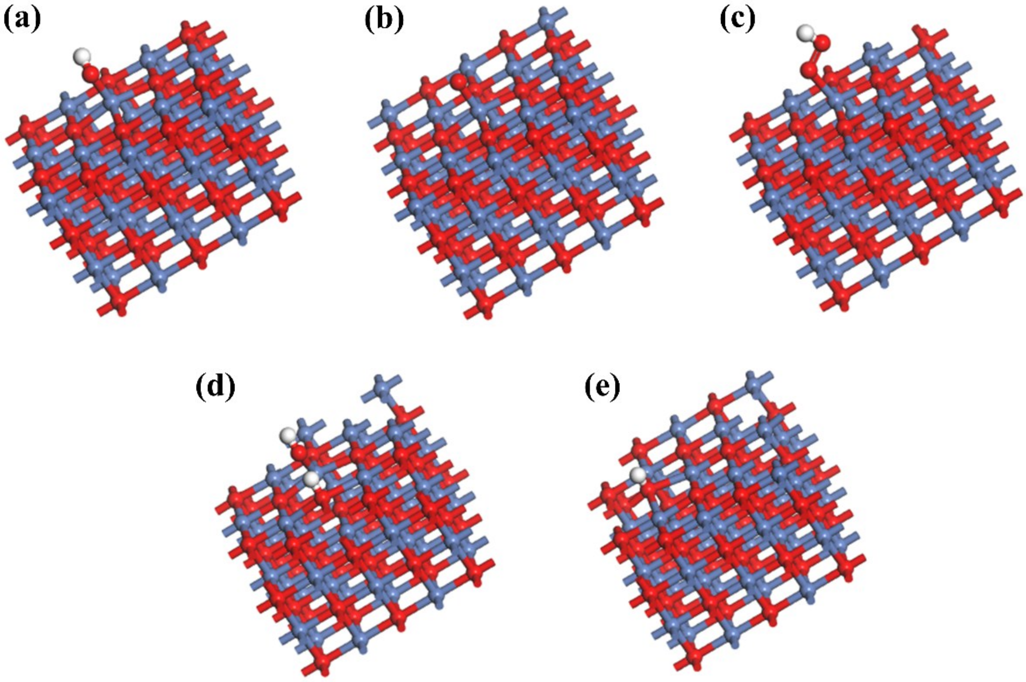

Figure S30 DFT models of NiO for a-c) OER with OH*, O* and OOH*, d,e) HER with H-OH and H*.

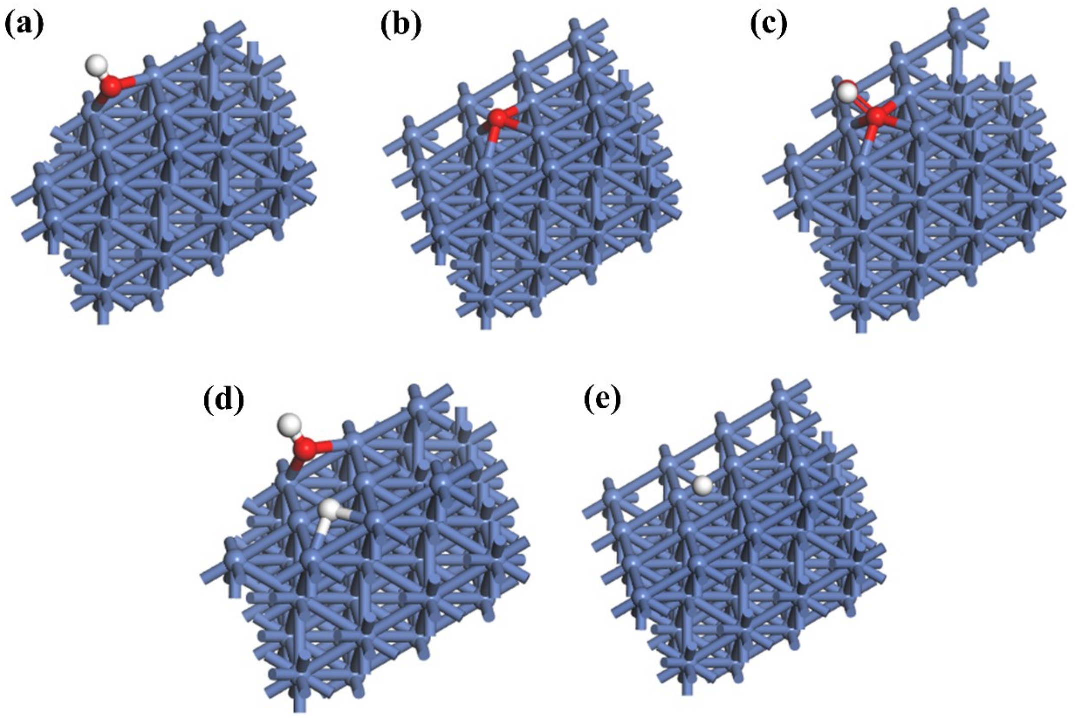

Figure S31 DFT models of Ni for a-c) OER with OH*, O* and OOH*, d,e) HER with H-OH and H*.

Table S1 Correction of zero point energy and entropy of the adsorbed and gaseous species.

	ZPE(eV)	TS(eV)
OOH*	0.35	0
O*	0.05	0
H*	0.16	0.01
OH*	0.31	0.01
H_2O	0.56	0.67
H_2	0.27	0.41

Table S2 Elements components in 1M KOH by ICP-OES.

	K (wt%)	Ca (wt%)	Al (wt%)	Na (wt%)	Ni (wt%)
1M KOH	99.06	0.003629	0.003069	0.9326	0.00053
After OER CV	99.08	0.002504	0.002956	0.9123	0.00053
After HER CV	99.10	0.003333	0.002917	0.08931	0.00052

Table S3 Comparison of OER performance.

Catalysts	η_{10} (mV)	References
2D/3D NiO DSE	230	This work
NiO_x	300	J. Am. Chem. Soc. 2012, 134, 17253
$Ni(OH)_2$	360	Energy Environ. Sci. 2016, 9, 1246
NiO/TiO_2	390	J. Am. Chem. Soc. 2016, 138, 6517.
Ni-Co Nanowires	302	Adv. Energy Mater. 2017, 7, 1601492
$CoNi(OH)_x$/Cu foil	280	Adv. Energy Mater. 2015, 6, 1501661
Ultrafine monolayer NiFe-LDH	254	Adv. Energy Mater. 2018, 8, 1703585
NiFe LDH Hollow prisms	280	Angew. Chem. Int. Ed. 2018, 57, 172
Ni_3S_2/NF	260	J. Am. Chem. Soc. 2015, 137, 14023
$Ni_2P_4O_{12}$/CC	280	Adv. Mater. 2018, 30,1705045

Table S4 Comparison of HER performance.

Catalysts	η_{10} (mV)	References
2D/3D NiO DSE	51	This work
V-doped Ni_3S_2	68	ACS Appl. Mater. Interfaces, 2017, 9, 59592.
Ni-$Ni(OH)_2$/CF	110	Nanoscale, 2018, 10, 17546
NiFeP/NiFe	255	ACS Appl. Mater. Interfaces, 2016, 8, 12798.
NiFe/$NiCo_2O^4$/NF	105	Adv. Funct. Mater., 2016, 26,3515
S-$NiFe_2O_4$/NF	138	Nano Energy, 2017, 40, 264
$NiCo_2O_4$	110	Angew. Chem. Int. Ed., 2016,55, 6290
Fe-CoP/Ti	78	Adv. Mater. 2017, 29, 1602441

Table S5 Comparison of overall water splitting performance.

Catalysts	Overall water splitting cell voltage (V @10mA/cm^2)	References
2D/3D NiO DSE	1.51	This work
NiCo-LDH/NF	1.66	Dalton Trans., 2017, 46, 8372
Co(OH)$_2$@NCNTs@NF	1.72	Nano Energy, 2018, 47, 96
NiCoP/NF	1.58	Nano Lett. 2016, 16,7718
NiCo$_2$O$_4$	1.65	Angew. Chem. Int. Ed., 2016, 128, 6398.
Ni@CNS@NF	1.57	J. Mater. Chem. A 2016, 4, 7297
Cu@NiFe LDHNF	1.54	Energy Environ. Sci.2017, 10, 1820
NiCoP/rGO	1.59	Adv. Funct. Mater. 2016, 26, 6785.

Movie S1

The overall water splitting of NiO-Vo@2D/3D NS@DSE.

References

1 Kresse, G. and J. Furthmüller, *Physical Review B*, 1996, **54**,11169.

2. Kresse, G. and J. Hafner, *Physical Review B*, 1994, **49**, 14251.
3. Blöchl, P.E., *Physical Review B*, 1994, **50**, 17953.
4. Perdew, J.P., K. Burke, and M. *Physical Review Letters*, 1996, **77**, 3865.
5. Zhang, Y. and W. Yang, *Physical Review Letters*, 1998, **80**, 890.
6. Hammer, B., L.B. Hansen, and J.K. Nørskov, *Physical Review B*, 1999, **59**, 7413.
7. Dudarev, S., et al., *Physical Review B*, 1998, **57**, 1505.
8. Monkhorst, H.J. and J.D. Pack, *Physical review B*, 1976, **13**, 5188.
9. Nørskov, J.K., et al., *The Journal of Physical Chemistry B*, 2004, **108**, 17886.
10. Rui Li, Xiongjun Liu, Ruoyu Wu, Jing Wang, Zhibin Li, K. C. Chan, Hui Wang,Yuan Wu, and Zhaoping Lu. *Adv. Mater.*, 2019, 10.1002/adma.201904989.